

RESEARCH ARTICLE

Added mass in rat plantaris muscle causes a reduction in mechanical work

Stephanie A. Ross^{1,*}, Barbora Rimkus², Nicolai Konow^{2,3}, Andrew A. Biewener³ and James M. Wakeling¹

ABSTRACT

Most of what we know about whole muscle behaviour comes from experiments on single fibres or small muscles that are scaled up in size without considering the effects of the additional muscle mass. Previous modelling studies have shown that tissue inertia acts to slow the rate of force development and maximum velocity of muscle during shortening contractions and decreases the work and power per cycle during cyclic contractions; however, these results have not yet been confirmed by experiments on living tissue. Therefore, in this study we conducted *in situ* work-loop experiments on rat plantaris muscle to determine the effects of increasing the mass of muscle on mechanical work during cyclic contractions. We additionally simulated these experimental contractions using a mass-enhanced Hill-type model to validate our previous modelling work. We found that greater added mass resulted in lower mechanical work per cycle relative to the unloaded trials in which no mass was added to the muscle ($P=0.041$ for both 85 and 123% increases in muscle mass). We additionally found that greater strain resulted in lower work per cycle relative to unloaded trials at the same strain to control for length change and velocity effects on the work output, possibly due to greater accelerations of the muscle mass at higher strains. These results confirm that tissue mass reduces muscle mechanical work at larger muscle sizes, and that this effect is likely amplified for lower activations.

KEY WORDS: Cyclic contractions, Inertia, Muscle mass, Muscle mechanics, Mechanical work, Skeletal muscle

INTRODUCTION

The behaviour of whole muscle is fundamental to human and animal movement. However, due to the difficulty in measuring whole muscle function in larger animals, most of what we know about the intrinsic properties that dictate this behaviour comes from studies on isolated preparations of single fibres or small muscles during controlled, maximal contractions. To predict the behaviour of larger whole muscles, we scale up these intrinsic properties of single fibres or small muscles as if we were scaling the force–length properties of a massless ideal spring to larger sizes (Zajac, 1989). As a result, the forces increase in proportion to the muscle's maximum isometric force (or cross-sectional area assuming constant


maximum isometric stress) and the lengths and velocities increase in proportion to the muscle's length. This method of scaling, which is used in nearly all Hill-type muscle models (e.g. Zajac, 1989; Thelen, 2003; Millard et al., 2013), assumes that the same mechanisms that dictate the behaviour of a single fibre also dictate the behaviour of whole muscle of any size. In other words, we assume that the non-dimensional behaviour of a 15 kg elephant muscle is the same as that of a 1 mg single fibre. Yet when we compare the output of these models with experimental measures of whole muscle, Hill-type models tend to perform quite poorly, particularly under conditions that differ from that of the maximal, controlled contractions used to measure the muscle's intrinsic properties (Perreault et al., 2003; Dick et al., 2017). Therefore, this method of scaling that assumes whole muscles behave the same as giant single fibres is not likely to account for all the mechanisms that underlie whole muscle behaviour.

Unlike an ideal spring, fibres and whole muscles have mass, and while the effects of this mass may be negligible for single fibres or small muscles, this may not be true for larger muscles. As muscles increase in size, their potential to generate force increases in proportion to their cross-sectional area, and their mass increases in proportion to their volume. This results in greater internal loads for larger muscles relative to the force that they can produce at any activation; however, this difference becomes greater when muscle force potential decreases during submaximal contractions, which are most relevant to *in vivo* motor behaviours (Shiavi and Griffin, 1983; Gillis and Biewener, 2001; McGuigan et al., 2009; Tikkanen et al., 2013). The effect of these internal inertial loads depends not only on the magnitude of the tissue mass but also the acceleration of that mass. Therefore, tissue inertia likely has the largest effect during submaximal contractions when muscle forces are low, and during unsteady or higher frequency or strain cyclic contractions when accelerations of the tissue are greatest. However, because the intrinsic force–velocity properties of muscle are taken primarily from measures on fully active single fibres or small muscles that have little mass, and under conditions in which the fibre or whole muscle acceleration is zero, the effects of these internal loads are not likely to be accounted for in the Hill-type model formulation. Ignoring the effects of muscle mass may therefore contribute to the discrepancies observed between Hill-type model predictions and experimental measures.

The effect of muscle tissue mass has rarely been studied and has primarily been provided only as a tentative explanation for experimental observations that could not be explained otherwise. In the late 1980s, Josephson and Edman (1988) compared the maximum shortening speed of fibre bundles to that of single fibres isolated from those same bundles and found that faster fibres contracted more slowly when they were within a fibre bundle than when they were in isolation. This result led the authors to suggest that faster fibres within whole muscle may contract more slowly because of the load provided by neighbouring fibres (Josephson and

¹Department of Biomedical Physiology and Kinesiology, Simon Fraser University, Burnaby, BC, V5A 1S6, Canada. ²Department of Biological Sciences, University of Massachusetts Lowell, Lowell, MA 01854, USA. ³Concord Field Station, Museum of Comparative Zoology and Department of Organismic and Evolutionary Biology, Harvard University, Bedford, MA 01730, USA.

*Author for correspondence (saross@sfu.ca)

 S.A.R., 0000-0003-3512-9579; B.R., 0000-0002-9095-8233; N.K., 0000-0003-3310-9080; A.A.B., 0000-0003-3303-8737; J.M.W., 0000-0003-0817-0867

Edman, 1988). Prior to this, whole muscle was assumed to be able to contract as fast as the fastest fibre within the muscle (Hill, 1970). More recently, Holt and colleagues showed that whole rat plantaris muscle contracts more slowly when only a portion of the fibres in the muscle are active compared with when the muscle is fully active, even if the active portion is composed entirely of fast fibres (Holt et al., 2014). The authors suggested that this effect is due to the inactive muscle tissue providing resistance to slow the contraction speed of the active fibres. Studies using a Hill-type model that accounts for tissue mass (Günther et al., 2012) have supported this conclusion and have shown that lower activation results in slower maximum contraction speeds (Ross and Wakeling, 2016), as does larger muscle mass (Meier and Blickhan, 2000; Böl and Reese, 2008; Ross and Wakeling, 2016). Furthermore, larger muscle mass has also been shown to decrease the mechanical work done and power generated during cyclic contractions (Ross et al., 2018a).

Despite these results from modelling studies, the effects of muscle mass have not yet been confirmed by experiments on living tissue. Therefore, in this study we conducted *in situ* work-loop experiments on rat plantaris muscle to determine the effects of increasing the internal mass of muscle on contractile performance, specifically mechanical work output per cycle. We also simulated the *in situ* experimental conditions using the mass-enhanced Hill-type muscle model (Günther et al., 2012; Ross and Wakeling, 2016; Ross et al., 2018a) to validate the results of the previous modelling studies.

MATERIALS AND METHODS

In situ experimental set-up

We collected data on the right plantaris muscle of seven male Sprague–Dawley rats [*Rattus norvegicus* (Berkenhout 1769); body mass: 416.3±31.9 g (mean±s.d.); approximate age: 3–4 months; Charles River, Wilmington, MA, USA]. All experiments were conducted at Harvard University's Concord Field Station in Bedford, MA, USA in accordance with the guidelines of the Faculty of Arts and Sciences Institutional Animal Care and Use Committee of Harvard University and the University Animal Care Committee of Simon Fraser University. Rats were kept under isoflurane anaesthesia, administered via a mask, for the duration of the experiment (3% induction, 1.5% maintenance). To allow us to externally stimulate the plantaris muscle, we placed a bipolar nerve cuff electrode around the sciatic nerve, which we accessed through the right lateral aspect of the thigh, and then cut the nerve proximal to the cuff to remove descending control of the muscle by the central nervous system.

To completely expose and isolate the plantaris muscle, we first opened and separated the skin and fascia of the medial aspect of the hindlimb from the underlying tissue using blunt dissection. We then cut the distal tendons of the medial and lateral gastrocnemii, soleus, tibialis anterior, and digit flexors and reflected those muscles to completely expose the plantaris and prevent effects from co-contraction of the surrounding musculature. To attach the muscle of interest to the servomotor (series 305B-LR, Aurora Scientific Inc., Aurora, ON, Canada), we tied Kevlar thread at the myotendinous junction and secured the knot with cyanoacrylate gel to minimise the potential effects of series elasticity and knot slippage. We then cut the distal end of the plantaris tendon near the calcaneus and tied the thread to the lever arm of the servomotor to connect the muscle to the motor. To fix the proximal end of the muscle, we secured the right hindlimb of the rat to a stereotaxic frame with a femur clamp and anchored the right foot to a metal plate attached to the frame. We maintained the temperature of the muscle at

approximately 30°C using a heat mat and lamp and kept the exposed tissue moist by regularly applying saline solution with a syringe. Following the experiments, we euthanised the deeply anaesthetised rats with an overdose (150 mg kg⁻¹) of intracardially injected pentobarbital sodium.

Experimental conditions

To determine the effects of tissue mass on muscle mechanical work, we conducted work-loop experiments where the muscle underwent cyclic length changes coupled with bursts of excitation timed to the phase of the contraction cycle. The area inside the work-loop created when the time-varying muscle force is plotted against muscle length gives the net mechanical work of the muscle per cycle [see Josephson (1985) for further details]. Muscles can produce a variety of different work-loop shapes depending on the requirements of the task and conditions of the external environment (Dickinson et al., 2000). In this study, we aimed to examine the effects of mass on muscle work during cyclic contractions in which the muscle behaves as a motor, with large positive work and a boxy counter-clockwise work-loop shape, to provide a comparison to our previous simulation work (Ross et al., 2018a). The mechanical work of a muscle depends on a number of factors, including the muscle's strain trajectory relative to its force–length properties, the muscle's velocity relative to its force–velocity properties, the pattern and phase of stimulation relative to the muscle's strain trajectory, and the cycle frequency (Josephson, 1993). To maximise mechanical work per cycle, we centred the muscle strain trajectory about optimal length, which we determined from the tetanic force–length relationship for each preparation, so that the muscle would produce high force by operating primarily on the plateau of its force–length curve. Additionally, we started stimulating the muscle slightly before the start of shortening (–5%), so that the muscle force would be high for the duration of the shortening phase (Johnson and Johnston, 1991; James et al., 1996). We also stimulated the muscle with a duty cycle of 0.4 so that the muscle would not be actively producing force during the lengthening phase of the cycle (Swoap et al., 1997). This resulted in a stimulation train duration of 200 ms for the 2 Hz frequency cycles (3 V supramaximal stimulus; 0.3 ms pulse width; 150 Hz pulse frequency; S48, Grass Technologies, West Warwick, RI, USA).

The effect of muscle mass on the mechanical work output of the muscle is due to a balance between the force the muscle can produce and the internal inertial loads it must accelerate. To manipulate this balance and alter the mass effects, we altered the muscle force, the magnitude of the internal muscle mass, and the muscle accelerations. To alter the muscle force, we conducted both active and passive work-loops, in which both the active and passive forces and only the passive forces contributed to the total muscle force, respectively. We used supramaximal stimulation for the active work-loops to activate all (or nearly all) of the muscle volume. Reducing the total muscle force by not activating the muscle should have a similar effect to reducing the active muscle force with submaximal contractions, where the work per cycle is lower due to relatively greater inertial loads (Ross et al., 2018a). To alter the accelerations of the muscle, we modified the strain amplitude of the sinusoidal trajectory that dictated the servomotor and muscle length changes during each trial. Increasing the magnitude of the muscle strain would increase the accelerations that the tissue mass experiences, and this in turn would alter the balance of internal forces and decrease the cyclic work output of the muscle. Although increasing the frequency of the contraction cycles would produce a similar effect to increasing the muscle strain, we chose to keep

frequency constant throughout the trials to control for reductions in muscle work that occur at higher frequencies due to longer activation and deactivation times relative to the duration of the cycle shortening phase (Caiozzo and Baldwin, 1997). To alter the mass properties of the muscle, we added effective mass by inserting an insect pin (no. 3; 0.5 mm diameter; stainless steel) through the cross-section of the muscle belly, midway along its length. This pin was fixed to one end of a movement arm that passively rotated depending on the force applied by the muscle to the pin (Fig. 1). A weight could be attached to the other end of the movement arm opposite to the pin to increase the effective mass of the muscle beyond what the movement arm alone would exert. The hollow carbon fibre movement arm rested on a cone-shaped component to reduce the area of contact with the movement arm and minimise the effects of friction (Fig. S1). We attached this set-up to add effective mass to the muscle to a micromanipulator on a magnetic stand (Kite Manual Micromanipulator and M10 Magnetic Stand, World Precision Instruments, Sarasota, FL, USA) to allow for fine adjustment of the position of the pin.

Each muscle underwent all combinations of two force conditions (active and passive), three strain conditions (± 5 , ± 7.5 and $\pm 10\%$ relative to optimal length, resulting in total shortening strain of 10%, 15% and 20%), and three mass conditions (unloaded, movement arm with no weight, and movement arm +1.1 g weight, resulting in an effective added mass of 0%, $84.9 \pm 7.5\%$ and $122.9 \pm 10.8\%$ muscle mass) twice for a total of 36 work-loops. We did not select the mean effective mass relative to the muscle mass but rather measured this value after the experiments were completed and the muscles were excised and weighed. We additionally conducted work-loop trials using a larger weight; however, this weight was

unstable on the movement arm and so these results are not reported in this paper. We blocked the work-loop trials by mass condition to reduce damage to the muscle from adjusting the pin attached to the movement arm. We then randomised these mass condition blocks to control for order effects, except for the unloaded condition which always occurred first to avoid disturbing the pin once it was placed in the muscle. Within each mass condition block, we conducted six work-loop trials (two force conditions \times three strain conditions) in random order. Between each work-loop trial containing five consecutive contraction cycles, we allowed the muscle to rest for 5 min, and between each block of work-loop trials, we conducted maximal tetanic contractions at optimal length to monitor the extent of muscle fatigue over the duration of the experiments. After we completed all blocks of work-loop trials, we repeated the trials a second time in reverse order to further control for fatigue and order effects. We terminated the trials when we saw visual changes in work-loop shape due to fatigue, such as prolonged relaxation times (Stevens and Syme, 1989, 1993; Askew et al., 1997) and decreased ability of the muscle to maintain force during shortening (Askew et al., 1997; Wilson and James, 2004). Likely due to our relatively low cycle frequency (Stevens and Syme, 1993) and 5 min recovery periods between trials, we did not see indicators of these changes in our muscle preparations. Additionally, we inspected the muscles post-mortem and found no evidence of discernible damage to the muscle tissue from the pin. For a visual of the experimental design, see Fig. S2.

Data collection and analysis

We measured output torque and position of the servomotor and the stimulus pulse delivered to the sciatic nerve in volts, and simultaneously generated the stimulus pulse at a sampling frequency of 4000 Hz using a custom-built virtual instrument and data acquisition board (Igor Pro version 7.0.8.1, Wavemetrics, Lake Oswego, OR, USA; USB-6259, National Instruments, Austin, TX, USA). We filtered the output data using a fourth-order Butterworth low-pass filter with a 55 Hz cut-off frequency and converted the output voltages to force (N) and length (m) using linear calibration curves. To determine the mechanical work per cycle of the muscle for each trial, we integrated the instantaneous mechanical power (product of muscle force and velocity) over the time duration of each cycle and then took the mean of the last three cycles. Then, to further control for the decrease in maximum muscle force over the duration of the experiments due to fatigue in addition to randomising and repeating trials, we normalised the mean mechanical work for each active work-loop trial by the approximate maximum tetanic muscle force at the time of the trial using a linear interpolation of the maximum tetanic force from the control contractions that occurred between each block of work-loops (Fig. S2) as a function of the trial number. Although we did not observe any obvious changes in work-loop shape during the experiments, we did see a mean reduction in maximum isometric force of 22% across all rats. A typical plot of the maximum isometric force from the control tetanic contractions over the duration of the trials can be seen in Fig. S3. We used a similar scheme to normalise the mechanical work from the passive work-loop trials but used the approximate passive force at optimal length at the time of the trial rather than the maximum tetanic force. Normalising the mechanical work per trial by muscle force resulted in normalised work with dimensions of length, so we also normalised the work by the given muscle's optimal length to result in dimensionless work. Finally, we took the mean work from the two repeated trials so that there was only one independent sample for each rat for each condition in the analysis. We conducted

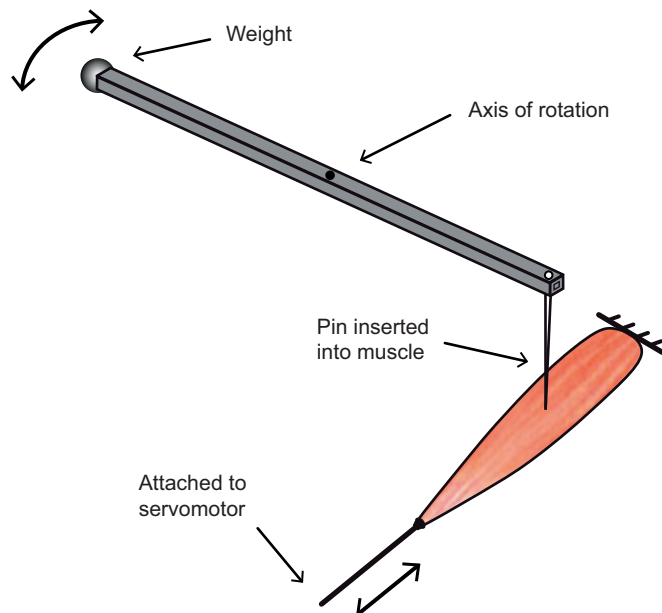


Fig. 1. Set-up to add effective mass to the *in situ* plantaris muscles. To add mass to the muscle, we developed a system in which a 1.9 g, 14 cm long hollow carbon fibre rod rotated about a pivot. On one end of the rod we attached an insect pin which we inserted into the muscle midway along its length, and on the other end we could attach weights of different sizes to add effective mass to the muscle acting through the pin. The proximal end of the muscle was fixed by securing the hindlimb of the rat to a stereotaxic frame with a femur clamp, and the distal end was tied to the lever arm of a servomotor. Vascular supply to the muscle remained intact and we externally stimulated the sciatic nerve innervating the plantaris using a bipolar nerve cuff electrode.

all post-processing in Mathematica (version 12, Wolfram Research, Champaign, IL, USA).

Statistical analysis

To examine the effects of added mass and strain amplitude on the mean mechanical work per cycle, we conducted repeated measures analysis separately for active and passive trials using a linear mixed model fit using maximum likelihoods with the function *lmer* in the package *lme4* (Bates et al., 2014) in R (version 3.6.1; <http://www.R-project.org/>). In the model, we included dimensionless mechanical work as a continuous response variable, strain and mass as categorical fixed effects, and subject as a categorical random effect. We did not include an interaction effect between strain and mass as it did not improve the model fit on initial tests. To examine the pairwise differences in mean mechanical work across all strain and mass conditions, we used the Holm–Bonferroni method (Holm, 1979) within the package *multcomp* (Hothorn et al., 2008) to control for the increase in family-wise error rate with multiple comparisons. We repeated this same analysis but with the dimensionless work normalised to the unloaded condition at the same strain as the continuous response variable to examine how strain alters the effects of added mass. In this analysis, we excluded the unloaded 0% added mass condition as there was no variance in the normalised work for these trials. All experimental results are reported as means±s.e.m.

Muscle model and simulations

To validate the Hill-type model accounting for tissue mass used in Ross and Wakeling (2016) and Ross et al. (2018a), and to confirm that our method of adding mass to the muscle is theoretically analogous to adding mass to the muscle model, we ran simulations with the mass-enhanced model to replicate the conditions of the *in situ* experiments in this study.

The mass-enhanced model used to predict the *in situ* muscle behaviour in this study has been described in detail elsewhere (Günther et al., 2012; Ross and Wakeling, 2016; Ross et al., 2018a). In brief, the model contains 16 point masses distributed evenly along the length of the muscle at rest to represent the mass of the muscle (Fig. 2). The mass of each point mass is equal to the total mass of the muscle divided by the number of point masses. Between the point masses are Hill-type muscle segments that produce force as a function of their activation, length and velocity. To model the

intrinsic force–velocity and force–length properties of muscle segments, we used Bézier curves (Ross et al., 2018b) fitted to experimental data from Roots et al. (2007) and Winters et al. (2011), respectively. Because the forces, lengths and velocities in these curves are dimensionless, and we used maximum isometric force F_0 , maximum intrinsic shortening velocity v_0 , and optimal length L_0 values that were specific to rat plantaris muscle, we effectively only fitted the dimensionless shape of the force–velocity and force–length curves. The model assumes that the muscle’s fibres are arranged in parallel, and as we controlled for the effects of the tendon during the *in situ* experiments by tying off the Kevlar string connecting the muscle to the servomotor directly at the myotendinous junction, we did not include a series elastic element in the model formulation. The properties of the model, such as the maximum isometric force, optimal length, and rate of activation, were taken as the mean values obtained from the *in situ* experiments (Table S1).

To increase the mass of the muscle model, we added mass to the point mass that was located at the average position of the pin along the length of the *in situ* muscle. To mimic the work-loop conditions of the *in situ* experiments, we constrained the end of the muscle model to follow a sinusoidal trajectory, and for conditions where the muscle was producing active force, we introduced a square wave excitation–time trace that reproduced the sciatic nerve stimulation in the experimental protocol. We then ran this excitation function through an excitation–activation transfer function (Zajac, 1989) to add delays between onset and peak activation and peak activation and complete deactivation. As in the *in situ* muscle experiments, we shifted the start of excitation 5% (25 ms) earlier in time relative to the start of shortening to maximise work per cycle. To examine the effects of muscle mass on the mechanical work of the muscle model, we replicated the *in situ* experimental conditions and varied the muscle force (active and passive), the effective mass added to the muscle model, and the strain amplitude of the contraction cycles. Due to our aim to minimise fatigue of the muscle preparations, in the experiments we were limited in the range of added mass and strain conditions we could examine. However, in the simulations we were able to extend the range of added masses to 400% muscle mass and strains to ±20% for a total shortening strain of 40%. We additionally ran simulations where the added mass was distributed evenly across all 16 point masses in the mass-enhanced model to confirm that the

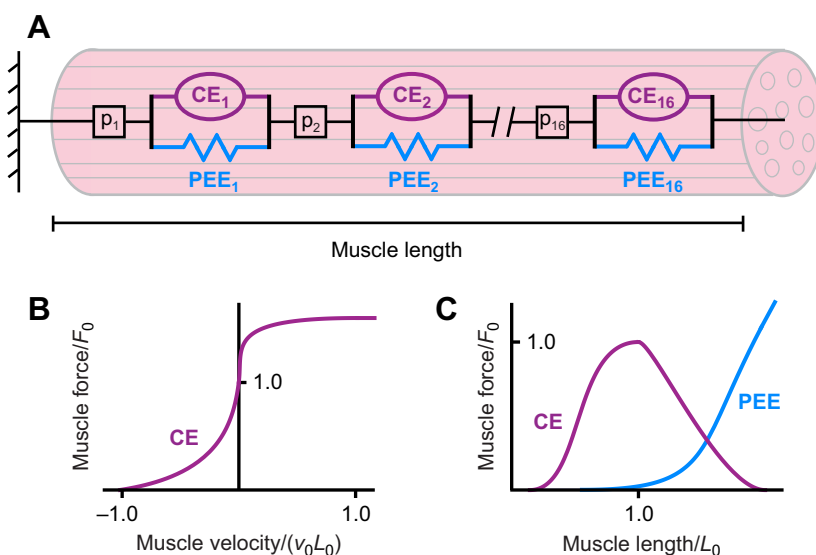


Fig. 2. Muscle model used to simulate experimental contraction cycles. (A) The mass of the muscle was distributed along the length of the model in a series of 16 point masses (p_1 – p_{16}). The point masses were separated by Hill-type actuators that each contained a contractile element (CE) and parallel elastic element (PEE). The force of the CE was due to its normalized force–velocity (B) and normalized force–length (C; purple) properties and the force of the PEE depended on only its normalized force–length properties (C; blue). The normalized force–velocity and normalized force–length properties were represented by Bézier curves developed in Ross et al. (2018a) and fitted to experimental data from Roots et al. (2007) and Winters et al. (2011), respectively. To replicate the *in situ* experimental work-loops, one end of the model was fixed and the other was constrained to follow a sinusoidal trajectory.

effects of adding mass to one point within the muscle are similar to distributing that added mass along the muscle's length. We conducted all simulations in Mathematica (version 12).

RESULTS

The mean mass, optimal length L_0 , maximum isometric force F_0 , and activation rate constant τ_{act} of the muscles examined in this study can be found in Table S1 and raw data for the *in situ* work-loop trials can be found in Table S2. For the active work-loop experiments, we started stimulating the sciatic nerve 25 ms before the start of the shortening period (-5% relative phase) where the muscle reached its longest length. This resulted in the muscle reaching peak force close to the start of shortening and then maintaining high forces for the duration of the shortening phase of the cycle (Fig. 3A). As a consequence of this behaviour, the mechanical work output per cycle of the muscle was positive and fairly large, resulting in counterclockwise work-loops that resembled that of a motor (Fig. 3A). To replicate this work-loop behaviour in the model simulations, we activated the muscle model using a time-varying excitation signal that was shifted in time so that, as with the *in situ* muscle experiments, the muscle excitation started 5% of the cycle duration before the start of the shortening phase. This resulted in simulated work-loops that were similar in shape to the experimental work-loop traces, except that the relaxation times were longer for the model simulations compared

with the rat plantaris contractions (Fig. 3B). We also conducted passive work-loop trials for the *in situ* experiments, in which the muscle length changes were identical to those for the active trials, except that the sciatic nerve was not stimulated and so active muscle force did not develop (Fig. 3C). These passive trials resulted in negative absolute work per cycle.

We found that greater added mass resulted in lower mechanical work per cycle for the active *in situ* work-loop trials (main effect: $P=0.021$; Fig. 4A). There was a $4.5\pm 1.9\%$ decrease in mean work per cycle between the unloaded (0% added mass) condition and the 85% added mass condition ($P=0.041$). When we increased the added mass to 123% of the muscle mass, the work decreased by $4.7\pm 1.9\%$ relative to the unloaded condition ($P=0.041$). We were unable to detect a difference in mechanical work per cycle between the 85% and 123% added mass conditions ($P=0.889$). For work-loops simulated with the muscle model, we found that increasing the mass of the muscle decreased its mechanical work output per cycle, similar to the *in situ* experiments. However, the magnitudes of the differences between the mass conditions were much smaller (less than 1%) in the simulated contraction cycles compared with what we found for the *in situ* experiments, so we chose to geometrically scale the muscle by a factor of 25 as per Ross et al. (2018b) to amplify these effects to within a comparable range of the experimental results. Because the geometric proportions of the model remained constant, muscle length scaled with the scaling factor, the cross-sectional area

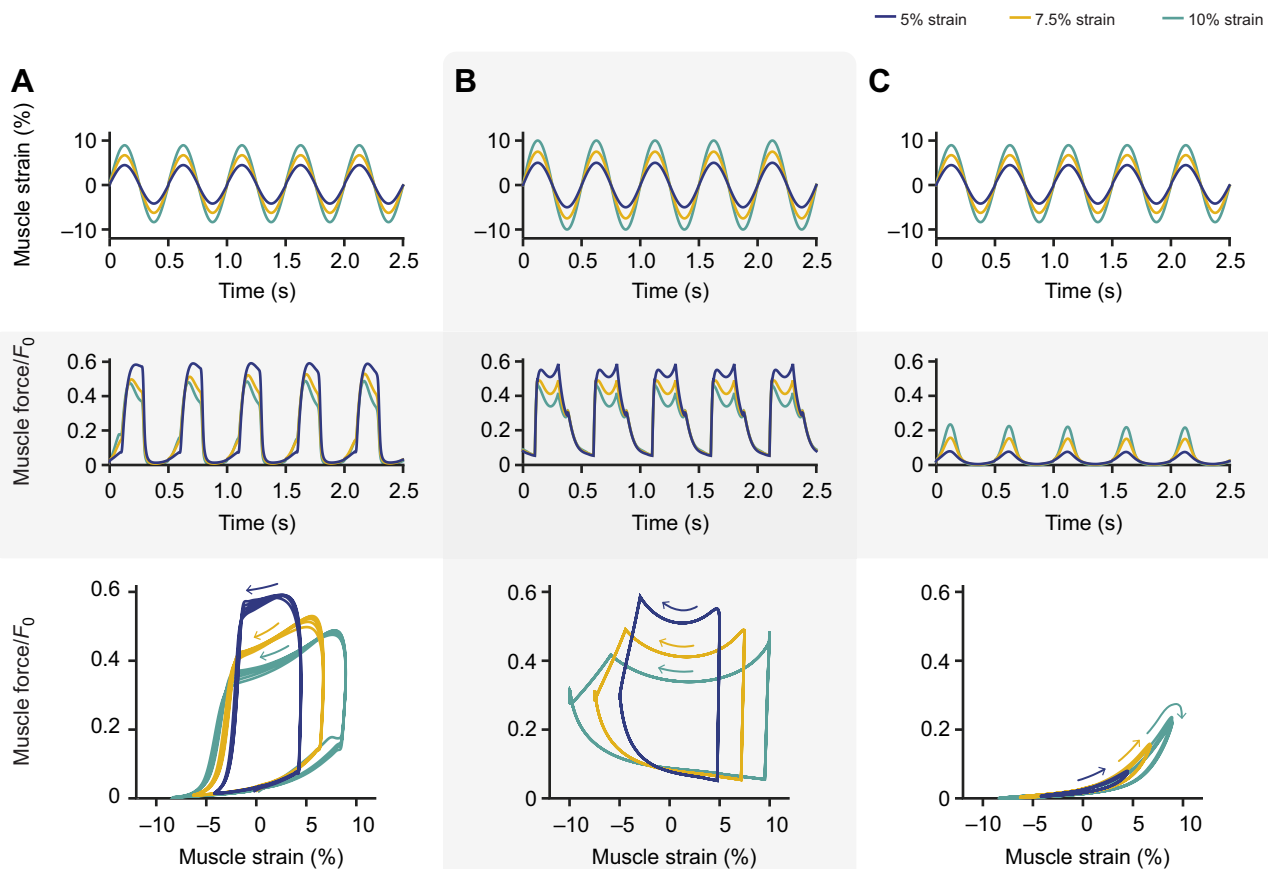


Fig. 3. Sample raw traces for unloaded trials at different strains. Raw traces for active contractions from *in situ* experiments (A) and simulations (B), and raw traces for passive simulations (C) are shown. The top row shows muscle strain over time, the middle row shows muscle force normalised to maximum isometric force (F_0) over time, and the bottom row shows the work-loops where normalised muscle force is plotted against muscle strain. Muscle strain is defined as the change in muscle length from optimal length (L_0) expressed as a percentage of optimal length. The raw traces are taken from representative unloaded (0% added mass) trials in a single rat at the three different strains.

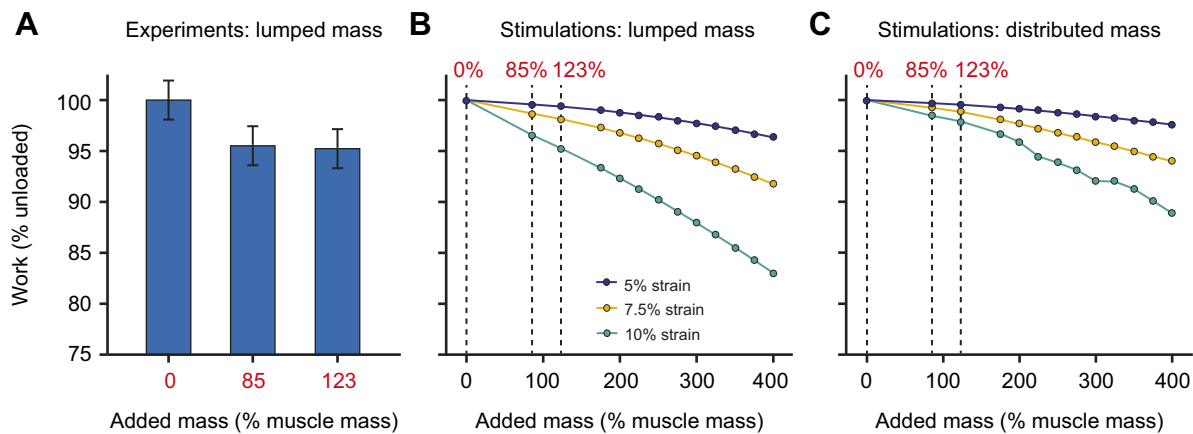


Fig. 4. Mass effects in active contractions. (A) The effect of added mass on normalised mean mechanical work per cycle ($P=0.021$) expressed as a percentage of the unloaded condition ($N=7$). Using *post hoc* analysis we were able to detect a difference between the 0% and 85% conditions ($P=0.041$) and the 0% and 123% conditions ($P=0.041$) but not between the 85% and 123% added mass conditions ($P=0.889$). Error bars are s.e.m. from the *post hoc* analysis. (B,C) Normalised mean work per cycle for lumped (B) and distributed (C) added mass simulations, where each point represents the work per cycle from a single simulation, for which we used the mean properties of the experimental muscles ($N=7$) as input parameters for the model. Added mass is expressed as a percentage of the mean muscle mass across all rats.

scaled with the square of the scaling factor, and the volume and tissue mass scaled with the cube of the scaling factor. As muscle maximum isometric force is proportional to the cross-sectional area, this scaling resulted in relatively larger muscle tissue mass relative to the maximum muscle forces. Conceptually, this scaling is akin to adding mass experimentally to the same size muscle. Further simulation results refer to this scaled model.

For simulations that mimicked the experimental set-up, where we added mass to the point mass closest to the average position of the pin inserted into the *in situ* muscle, we found that the mean mechanical work per cycle decreased by 1.7 and 2.4% for 85 and 123% added mass, respectively, across all three strain conditions (Fig. 4B). For simulations where we evenly distributed the added mass across all 16 point masses in the model, we found that the mean work per cycle decreased by 0.9 and 1.2% for 85 and 123% added mass relative to the unloaded condition, respectively, across all three strain conditions (Fig. 4C). For both these lumped and distributed added mass simulations, there was a greater reduction in mechanical work per

cycle with greater cycle strain, and the magnitude of this work reduction was greater for the lumped added mass simulations that mimicked the set-up of the *in situ* experiments. For the passive *in situ* work-loops where the nerve innervating the muscle was not stimulated, we were unable to detect an effect of added mass on mean mechanical work per cycle ($P=0.078$).

For the active *in situ* work-loop trials, we found that greater cycle strain led to greater work; however, when the work for each condition was normalised to the unloaded (0% added mass) condition at the same strain, we found that greater cycle strain resulted in lower mean mechanical work per cycle for the added mass conditions (main effect: $P=0.003$; Fig. 5A). Comparing between conditions, we found that mean work per cycle relative to the unloaded trials decreased by $4.8\pm 1.4\%$ between the 5 and 10% strain conditions ($P=0.002$) and $1.8\pm 1.4\%$ between the 5 and 7.5% strain conditions; however, this difference was not significant ($P=0.204$). Additionally, we were unable to detect a significant difference between the 7.5 and 10% strain conditions ($P=0.071$).

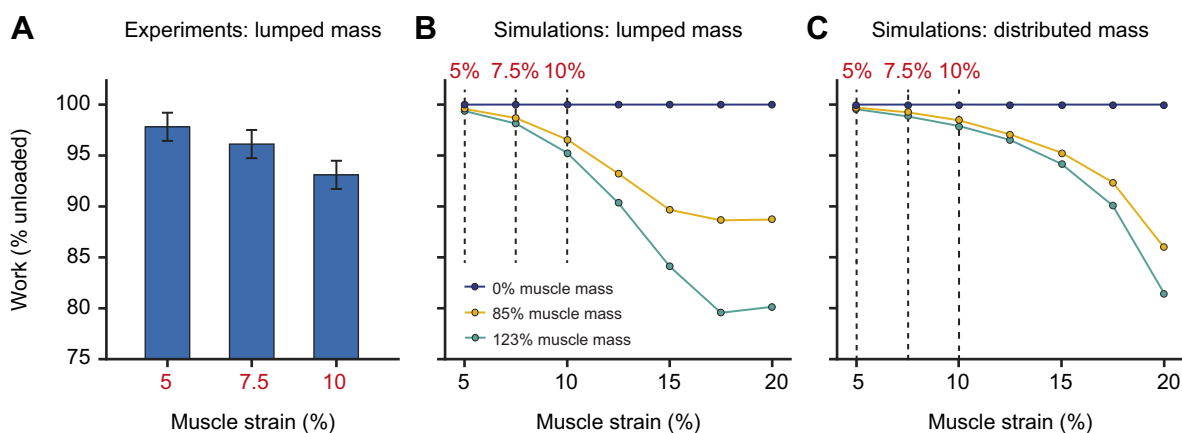


Fig. 5. Strain effects in active contractions. (A) The effect of muscle strain on normalised mean mechanical work per cycle relative to the unloaded condition at the same strain ($P=0.003$; $N=7$). Using *post hoc* analysis we were able to detect a difference between the 5 and 10% strain conditions ($P=0.002$), but not between the 5 and 7.5% conditions ($P=0.204$) or between the 7.5 and 10% conditions ($P=0.071$). The error bars are s.e.m. from the *post hoc* analysis. (B,C) Normalised mean work per cycle for lumped (B) and distributed (C) added mass simulations, where each point represents the normalised work per cycle from a single simulation where we used the mean properties of the experimental muscles ($N=7$) as input parameters for the model. Muscle strain is defined as the change in muscle length from optimal length (L_0) expressed as a percentage of optimal length.

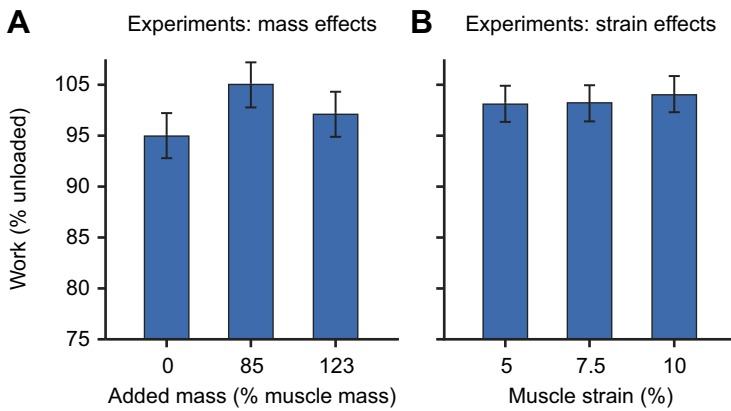


Fig. 6. Mass and strain effects on passive *in situ* muscle. Mean normalised work per cycle relative to unloaded across added mass (A) and strain (B) conditions. We were not able to detect a significant effect of either mass ($P=0.078$) or strain ($P=0.834$) on the mean work per cycle normalised to the unloaded condition at the same strain for the passive work-loop trials ($N=7$). The absolute work per cycle was negative for all passive trials, so mean work relative to unloaded greater than 100% indicates that the absolute work was negative and larger in magnitude than that for the unloaded condition. Error bars are s.e.m. from the *post hoc* analysis.

For the model simulations where the added mass was lumped near the centre of the muscle, we found that mean work per cycle relative to unloaded decreased by 1.1 and 3.6% for 7.5 and 10% strain, respectively, across the 85 and 123% added mass conditions (Fig. 5B). For both the simulations where the added mass was lumped and where it was distributed along the muscle's length, we found a greater reduction in work per cycle with greater strain relative to the unloaded condition (Fig. 5B,C). This reduction in work was greater in the lumped added mass simulations, except for the highest (20%) strain where we found the work reduction to be greater for the distributed mass simulations (Fig. 5C). As with the mass effects, we were unable to detect an effect of strain on the muscle mechanical work per cycle relative to the unloaded trials for the passive *in situ* work-loops where the muscle was not activated ($P=0.834$; Fig. 6B).

DISCUSSION

Most studies that examine the contractile properties of skeletal muscle focus on single fibres, fibre bundles, or small muscles for which the effects of muscle tissue inertia are largely negligible. As a consequence, we often assume that whole muscles behave as a scaled version of these single fibres or fibre bundles without considering the effects of the additional muscle tissue mass. However, modelling studies have shown that accounting for muscle mass can act to decrease maximum shortening velocities (Meier and Blickhan, 2000; Böl and Reese, 2008; Ross and Wakeling, 2016) and mechanical work per cycle (Ross et al., 2018a). While muscle mass can alter the behaviour of smaller or maximally active muscles, these effects are amplified by submaximal activation levels (Ross and Wakeling, 2016) and scaling muscle to larger sizes (Günther et al., 2012; Ross and Wakeling, 2016; Ross et al., 2018a). Despite these findings, as with any mathematical model, the models used in these studies are only a representation of the actual system of interest. Consequently, it is important to confirm that these mass effects occur in real muscle. Therefore, in this study we examined the effects of muscle tissue mass on the mechanical work per cycle of *in situ* rat plantaris muscle during both active and passive cycles of muscle length change (Fig. 3). To alter the effects of tissue inertia, we added effective mass to the muscle (Fig. 1) and we also varied the amplitude (strain) of the contraction cycles. The effects of tissue inertia depend on the magnitude of mass as well as the acceleration of that mass. Increasing the effective mass of the muscle acting through the pin and increasing the amplitude of the sinusoidal length changes increase the inertial loads within the muscle by increasing the magnitude of the mass and its acceleration, respectively. We hypothesised that an increase in internal inertial loads would

decrease net muscle force and, therefore, the work that the muscle would generate over a contraction cycle.

Mass effects in active contractions

We found that for active work-loop trials of the *in situ* muscle, the mean mechanical work per cycle decreased by 4.5 and 4.7% for an increase in effective mass of 85 and 123%, respectively (Fig. 4A). Although increasing the effective mass of muscle by 85 and 123% may seem quite large, these magnitudes are fairly small relative to the effective mass of inactive tissue that acts as an inertial load on actively contracting tissue during submaximal contractions. At the around 20% activation levels that muscles typically operate at during daily locomotion, such as level walking (Shiavi and Griffin, 1983; Gillis and Biewener, 2001; McGuigan et al., 2009; Tikkanen et al., 2013), the remaining inactive 80% of the muscle tissue would exert an inertial load with 400% effective mass against which active muscle fibres must contract. Increasing the effective mass by 85 and 123% during maximal contractions, as we did in this study, in theory represents inertial loads applied to the actively contracting muscle as if approximately 54 and 45%, respectively, of the muscle tissue were active [% active mass/(% active mass+% inactive or added mass), e.g. $100/(100+85)\approx 54$]. Therefore, the reductions in muscle work with greater added mass that we found in this study likely underestimate the reductions in work due to the inertia of inactive tissue that occur during daily activities.

In this study, we initially simulated the experimental contraction regimes using a Hill-type muscle model that accounts for tissue mass (Fig. 2C), where the dimensions of the muscle model were identical to those taken from the mean dimensions of the experimental muscle (a scale of 1). However, while these simulations resulted in lower work per cycle for greater mass, the magnitude of these effects were much smaller than what we saw for the *in situ* experiments. Therefore, we chose to scale the muscle model to a larger size (geometrically by a factor of 25) to amplify the mass effects to within the same order of magnitude as the experimental results. By doing so, we were able to determine if added mass resulted in the same pattern of effects on work for the *in situ* experiments as for the simulations. Additionally, the experimental conditions did not span the full range of mass effects that could be expected physiologically, and so the model provided a means to explore the more complete physiological range. For these scaled simulations with the added mass lumped as a point mass closest to the mean position of the pin inserted into the *in situ* muscle, we found that work decreased by 1.7 and 2.4% for 85 and 123% added mass, respectively, compared with the unloaded condition (Fig. 4B).

Potential differences between the intrinsic properties of the muscle model and the *in situ* rat plantaris muscle may have led to smaller reductions in work with greater added mass for the rat plantaris scale simulations compared with the *in situ* work-loop trials. First, because we did not measure the intrinsic force–velocity or full force–length properties of the *in situ* muscles in this study to minimise fatigue, and because no complete data sets are available describing these properties of the rat plantaris over the entire physiological range of muscle lengths (short to long) and velocities (shortening and lengthening), we fitted the force–length and force–velocity curves (Ross et al., 2018b) to data from rabbit tibialis anterior muscle (Winters et al., 2011) and intact rat flexor hallucis brevis fibre bundles (Roots et al., 2007), respectively. Therefore, these fitted curves may not entirely reflect the intrinsic properties of the rat plantaris. However, because we normalised the muscle and fibre bundle forces, lengths and velocities before we fitted the intrinsic curves to the data (Fig. 2B,C), and used F_0 , L_0 , and v_0 values that were specific to rat plantaris muscle in the model (Table S1), the fitted force–velocity and force–length curves likely did not vary substantially from that of the experimental muscles. Second, we did not incorporate history-dependent effects, such as force enhancement due to active lengthening (Abbott and Aubert, 1952; Cavagna and Citterio, 1974; Edman et al., 1982; Morgan et al., 2000; Herzog and Leonard, 2002) and force depression due to active shortening (Abbott and Aubert, 1952; Maréchal and Plaghki, 1979; Meijer et al., 1998; Herzog et al., 2000; Morgan et al., 2000) in our model formulation. Because these history-dependent effects are thought to be due to mechanisms at the crossbridge level (Herzog et al., 2012) and are not directly affected by the dynamics of muscle mass, their exclusion from the model formulation likely did not alter the main conclusions of the modelling results. Third, we determined only the activation rate constant in the Zajac (1989) excitation–activation transfer function from the experimental data. To determine the deactivation rate constant, we used a ratio β between the activation and deactivation rate constants of 0.6 (Dick et al., 2017), which resulted in prolonged relaxation times for the muscle model (Fig. 3B) relative to the rat plantaris muscles (Fig. 3A). However, while increasing β decreased the model relaxation times and resulted in work-loops that were closer in shape to the *in situ* muscle work-loops, changing β did not alter the added mass effects. Therefore, these features of the mass-enhanced muscle model likely did not contribute to the smaller reductions in work with greater added mass for the rat plantaris scale simulations compared with the *in situ* work-loop trials.

One-dimensional (1D) Hill-type muscle models fail to account for the three-dimensional (3D) shape and architecture of muscle, and this may have contributed to the discrepancy between the simulated and measured mass effects. When a muscle contracts and shortens it must bulge in width and thickness in order to maintain nearly constant volume (Baskin and Paolini, 1967). In pennate muscle, where the muscle fibres are oriented at an angle relative to the muscle line-of-action, the fibres can also rotate to greater angles as the muscle contracts (Gans and Bock, 1965; Fukunaga et al., 1997; Maganaris et al., 1998; Azizi et al., 2008; Randhawa et al., 2013). Because muscle fibres can rotate, they can shorten at different speeds relative to the muscle belly in a process known as architectural gearing (Azizi et al., 2008). The rat plantaris, examined here, is considered unipennate with a fibre pennation angle of 15–16 deg (Roy et al., 1982; Eng et al., 2008) relative to the muscle line-of-action at rest. Therefore, muscle shape change (e.g. bulging in thickness and width) and architectural gearing likely influenced the cyclic work-loop contractions studied in our experiments.

However, the mass-enhanced Hill-type model we used to simulate these contraction regimes is 1D and so only accounts for the muscle dynamics and kinematics along the muscle's length and does not account for the effects of tissue mass in other directions. Studies using 3D finite element models of muscle have shown that accounting for the effects of tissue mass in 3D can reduce maximum shortening velocity (Meier and Blickhan, 2000; Böl and Reese, 2008) and mechanical work per cycle (Ross et al., 2018a), similar to our previous 1D simulation results (Ross and Wakeling, 2016; Ross et al., 2018a). While no direct comparisons have yet been made between the magnitudes of the mass effects in 1D versus 3D, accounting for the effects of tissue mass in all directions, even in parallel-fibred muscles, would be likely to further reduce muscle work output per cycle, as greater internal work would be done to accelerate the tissue mass in transverse directions as the muscle shortens. The effects of tissue mass could be altered further in pennate muscle where the fibres can rotate relative to the line-of-action as well as change length. In our experiments, inserting the pin through the muscle along the plane perpendicular to the aponeuroses could have, to some extent, restricted changes in muscle shape and fibre rotations and altered the mechanical work output that we measured during the *in situ* experiments. Given these considerations, further work is needed to understand the 3D effects of tissue mass on whole muscle behaviour.

To confirm that adding mass to one point within the muscle results in similar effects to having that same added mass distributed along the muscle's length, we conducted additional simulations with the mass-enhanced Hill-type model but distributed the added mass evenly across all 16 point masses in the model. These simulations resulted in smaller mass effects compared with when the added mass was lumped into a single point mass midway along the muscle's length (Fig. 4B,C). While the mass of real muscle is continuous throughout its volume, we had to discretise the mass in our model using a series of point masses to approximate the dynamics of the system. While increasing the number of point masses gives a closer approximation to the behaviour of the continuous mass, the computational time substantially increases and, beyond 16 point masses, the increased accuracy from more point masses becomes insignificant (Günther et al., 2012). For our *in situ* rat plantaris experiments, we added effective mass to only a single location midway along the muscle's length to avoid altering the integrity of the muscle tissue. Therefore, the lumped added mass simulations and *in situ* experiments provide a coarse approximation of the change in inertial effects due to increasing muscle mass or decreasing activation during submaximal contractions. While the distributed added mass simulations better approximate the effects of continuous mass distributed throughout the volume of a muscle, few if any real muscles have their volume or mass distributed evenly along their length. Studies quantifying muscle architecture of human leg muscles using magnetic resonance imaging have shown that muscle cross-sectional area is largest towards the midpoint along the muscle's length and then tapers off towards the proximal and distal ends, but the location of this largest cross-sectional area differs between muscles (Fukunaga et al., 1992; Morse et al., 2007; Erskine et al., 2009; Cotofana et al., 2010; Maden-Wilkinson et al., 2013) and can change with active contraction (Hodgson et al., 2006). The inertia of inactive tissue during submaximal contractions are also not likely to be distributed evenly along the muscle's length due to regional variations in muscle activation (English, 1984; Pratt and Loeb, 1991; Boggs and Dial, 1993; Schieber, 1993; Soman et al., 2005; Wakeling, 2008; Kinugasa et al., 2011; Hodson-Tole

et al., 2013). Thus, the complexity of the inertial properties of *in vivo* muscle are likely not entirely captured by either the lumped or distributed added mass simulations.

Strain effects in active contractions

The mechanical work performed by a muscle over a contraction cycle depends on the pattern of muscle force in relation to the length change. If force is produced during shortening, increasing the cycle strain amplitude may be expected to increase work per cycle. However, because greater strain amplitude at constant cycle frequency increases the average shortening velocity of the muscle, greater strain could alternatively decrease work by decreasing muscle force due to force–velocity effects (Hill, 1938). Therefore, maximal work per cycle typically occurs at intermediate cycle strains (Josephson, 1985; Josephson and Darrell, 1989; Askew and Marsh, 1997). We found here that greater cycle strain led to greater mean absolute work per cycle, indicating that the rat plantaris was operating at small enough strains where reductions in force due to faster shortening speeds did not outweigh increases in work due to greater length change. In this study we were interested in using strain to manipulate the effects of inertia on muscle work by altering the accelerations of the muscle tissue and added effective mass. We expected that increasing the strain amplitude imposed by the servomotor would increase the accelerations of the muscle tissue mass and decrease mechanical work output per cycle. Indeed, we found that this was the case for the active contraction cycles when work was normalised to the unloaded (0% added mass) condition at the same strain to control for length change and velocity effects on the work output (Fig. 5).

Studies comparing Hill-type model predictions to *in situ* and *in vivo* muscle force measures show that these massless 1D models perform best during slow, maximal contractions and are least accurate when predicting faster, submaximal contractile conditions. Perreault and colleagues (2003) compared Hill-type forces with *in situ* cat soleus forces during contractions that mimicked *in vivo* length trajectories and found that errors exceeded 50% when the muscle strains were large and motor unit firing rates were low. Millard and coworkers (2013) showed that Hill-type model errors increased when predicting *in situ* cat soleus muscle forces during submaximal contractions (Perreault et al., 2003) compared with maximal contractions (Krylow and Sandercock, 1997). Similar results have been reported for larger animals: Wakeling and others (2012) found that the correlations between predicted and measured forces of *in situ* goat medial gastrocnemius were lower for lower stimulus frequency, and Dick and colleagues (2017) showed that Hill-type prediction errors of human medial and lateral gastrocnemius forces during cycling were lowest for low speed, high force contractions and increased with higher cadences. The results of the present study, along with our previous simulation work (Ross and Wakeling, 2016; Ross et al., 2018a), indicate that the effects of muscle mass are greatest during the higher strain and submaximal contractions where traditional massless Hill-type models perform the worst. Therefore, accounting for tissue mass may be a promising avenue to improve the predictive power of these widely used muscle models.

In this study we only examined sinusoidal length changes with supramaximal nerve stimulus to activate all or nearly all of the muscle fibres. We also used a stimulus duty cycle of 0.4 so that the muscle would generate active force for the majority of the cycle shortening phase to maximise work output. However, muscle behaviour during *in vivo* contraction cycles can vary widely depending on the muscle and the task. Therefore, further work is

needed to investigate how tissue inertia alters the behaviour of muscle across a wider range of activation and muscle length change patterns.

Passive muscle length changes

We were unable to detect an effect of either mass or strain during the passive work-loop trials (Fig. 6). Given that the magnitudes of work we measured during the cycles of passive length change were small relative to the magnitudes of work during the active contractions, it is likely that the effects of mass and strain under passive conditions were too small to detect given the variability among subjects and experimental noise in the data. When we simulated the passive work-loop conditions with the mass-enhanced muscle model, the point masses within the model oscillated at much higher frequencies than the cycle frequency, indicating that the system was unstable. This was not an issue for simulations involving active contractions because the concentric portion of the force–velocity relationship provides damping to stabilise the system and prevent the high-frequency oscillations of the point masses. In contrast, because the passive force of the muscle segments between the point masses depended only on length, there were no velocity-dependent damping effects to stabilise the model point masses during the passive work-loop simulations.

Viscous (velocity-dependent) damping has been described or discussed in studies of skeletal muscle (Gasser and Hill, 1924; Levin and Wyman, 1927; Heerkens et al., 1987; Syme, 1990; Best et al., 1994), as well as a range of other biological tissues, including cardiac muscle (Templeton and Nardizzi, 1974; Templeton et al., 1974), aponeuroses and tendons (Lieber et al., 2000; Maganaris and Narici, 2005), and fat (Chan and Titze, 1998; Schoemaker et al., 2006). Without the effects of viscosity, muscle would behave as a non-linear spring during passive length changes and return as much energy during shortening as it stores during lengthening. However, all the passive work-loops in this study resulted in negative work per cycle (Fig. 3C), indicating that energy was likely dissipated due to viscous damping. Except for a few studies that have incorporated viscous damping in parallel to the contractile element of muscle models to mimic the effects of viscosity within muscle tissue (Hatze, 1977; Günther et al., 2007), or to improve the numerical stability of the modelling computations and satisfy the balance of in-series forces between muscle and tendon (Millard et al., 2013), the effects of viscosity are typically neglected in the formulation of Hill-type muscle models. While viscous damping alone may have a negligible effect on muscle output forces, lengths and velocities, it could play an important role in dissipating energy and stabilising the mass of *in vivo* muscle tissue.

Conclusions

The purpose of this study was to determine the effects of altering the mass of *in situ* muscle on mechanical work during cyclic contractions. We found a statistically significant main effect of added mass on mechanical work per cycle. The condition with the greatest added mass resulted in the lowest work relative to the unloaded condition. We additionally detected a significant main effect of cycle strain, with the greatest strain condition resulting in the lowest work relative to the unloaded condition. We were able to replicate similar results to those of the *in situ* experiments in simulations of the mass-enhanced Hill-type model, but the magnitude of these effects was smaller. Because of the difficulty of measuring whole muscle function in living animals, we often rely on Hill-type muscle models to predict and understand whole muscle behaviour. However, these models, which rarely account for the

effects of muscle mass, have limited accuracy when predicting faster, higher strain, and submaximal contractions where the effects of muscle mass are likely to be greatest. Therefore, accounting for muscle mass may be a promising avenue to improve the predictive power of Hill-type muscle models and improve our understanding of whole muscle function in living animals.

Acknowledgements

We would like to thank P. Ramirez for animal husbandry and the anonymous reviewers for their feedback on the manuscript.

Competing interests

The authors declare no competing or financial interests.

Author contributions

Conceptualization: S.A.R., J.M.W.; Methodology: S.A.R., J.M.W.; Software: S.A.R.; Validation: S.A.R.; Formal analysis: S.A.R.; Investigation: S.A.R., B.R., N.K.; Resources: N.K., A.A.B., J.M.W.; Data curation: S.A.R.; Writing - original draft: S.A.R.; Writing - review & editing: S.A.R., B.R., N.K., A.A.B., J.M.W.; Visualization: S.A.R.; Supervision: N.K., A.A.B., J.M.W.; Funding acquisition: A.A.B., J.M.W.

Funding

This work was supported by a National Institutes of Health grant to A.A.B. and J.M.W. [2R01AR055648], a Natural Sciences and Engineering Research Council of Canada Discovery Grant to J.M.W. [RPGIN-2015-03966], and an Alexander Graham Bell Canada Graduate Scholarship-Doctoral to S.A.R. Deposited in PMC for release after 12 months.

Supplementary information

Supplementary information available online at <https://jeb.biologists.org/lookup/doi/10.1242/jeb.224410.supplemental>

References

- Abbott, B. C. and Aubert, X. M.** (1952). The force exerted by active striated muscle during and after change of length. *J. Physiol.* **117**, 77-86. doi:10.1113/jphysiol.1952.sp004755
- Askew, G. N. and Marsh, R. L.** (1997). The effects of length trajectory on the mechanical power output of mouse skeletal muscles. *J. Exp. Biol.* **200**, 3119-3131.
- Askew, G. N., Young, I. S. and Altringham, J. D.** (1997). Fatigue of mouse soleus muscle, using the work loop technique. *J. Exp. Biol.* **200**, 2907-2912.
- Azizi, E., Brainerd, E. L. and Roberts, T. J.** (2008). Variable gearing in pennate muscles. *Proc. Natl. Acad. Sci. USA* **105**, 1745-1750. doi:10.1073/pnas.0709212105
- Baskin, R. J. and Paolini, P. J.** (1967). Volume change and pressure development in muscle during contraction. *Am. J. Physiol.* **213**, 1025-1030. doi:10.1152/ajplegacy.1967.213.4.1025
- Bates, D., Mächler, M., Bolker, B. and Walker, S.** (2014). Fitting linear mixed-effects models using lme4. *J. Stat. Software* **67**, 1-48. doi:10.18637/jss.v067.i01
- Best, T. M., McElhaney, J., Garrett, W. E., Jr and Myers, B. S.** (1994). Characterization of the passive responses of live skeletal muscle using the quasi-linear theory of viscoelasticity. *J. Biomech.* **27**, 413-419. doi:10.1016/0021-9290(94)90017-5
- Boggs, D. F. and Dial, K. P.** (1993). Neuromuscular organization and regional EMG activity of the pectoralis in the pigeon. *J. Morphol.* **218**, 43-57. doi:10.1002/jmor.1052180104
- Böl, M. and Reese, S.** (2008). Micromechanical modelling of skeletal muscles based on the finite element method. *Comput. Methods Biomech. Biomed. Engin.* **11**, 489-504. doi:10.1080/10255840701771750
- Caiozzo, V. J. and Baldwin, K. M.** (1997). Determinants of work produced by skeletal muscle: potential limitations of activation and relaxation. *Am. J. Physiol.* **273**, C1049-C1056. doi:10.1152/ajpcell.1997.273.3.C1049
- Cavagna, G. A. and Citterio, G.** (1974). Effect of stretching on the elastic characteristics and the contractile component of frog striated muscle. *J. Physiol.* **239**, 1-14. doi:10.1113/jphysiol.1974.sp010552
- Chan, R. W. and Titze, I. R.** (1998). Viscosities of implantable biomaterials in vocal fold augmentation surgery. *Laryngoscope* **108**, 725-731. doi:10.1097/00005537-199805000-00019
- Cotofana, S., Hudelmaier, M., Wirth, W., Himmer, M., Ring-Dimitriou, S., Sängler, A. M. and Eckstein, F.** (2010). Correlation between single-slice muscle anatomical cross-sectional area and muscle volume in thigh extensors, flexors and adductors of perimenopausal women. *Eur. J. Appl. Physiol.* **110**, 91-97. doi:10.1007/s00421-010-1477-8
- Dick, T. J. M., Biewener, A. A. and Wakeling, J. M.** (2017). Comparison of human gastrocnemius forces predicted by Hill-type muscle models and estimated from ultrasound images. *J. Exp. Biol.* **220**, 1643-1653. doi:10.1242/jeb.154807
- Dickinson, M. H., Farley, C. T., Full, R. J., Koehl, M. A. R., Kram, R. and Lehman, S.** (2000). How animals move: an integrative view. *Science* **288**, 100-106. doi:10.1126/science.288.5463.100
- Edman, K. A., Elzinga, G. and Noble, M. I.** (1982). Residual force enhancement after stretch of contracting frog single muscle fibers. *J. Gen. Physiol.* **80**, 769-784. doi:10.1085/jgp.80.5.769
- Eng, C. M., Smallwood, L. H., Rainiero, M. P., Lahey, M., Ward, S. R. and Lieber, R. L.** (2008). Scaling of muscle architecture and fiber types in the rat hindlimb. *J. Exp. Biol.* **211**, 2336-2345. doi:10.1242/jeb.017640
- English, A. W.** (1984). An electromyographic analysis of compartments in cat lateral gastrocnemius muscle during unrestrained locomotion. *J. Neurophysiol.* **52**, 114-125. doi:10.1152/jn.1984.52.1.114
- Erskine, R. M., Jones, D. A., Maganaris, C. N. and Degens, H.** (2009). *In vivo* specific tension of the human quadriceps femoris muscle. *Eur. J. Appl. Physiol.* **106**, 827. doi:10.1007/s00421-009-1085-7
- Fukunaga, T., Ichinose, Y., Ito, M., Kawakami, Y. and Fukashiro, S.** (1997). Determination of fascicle length and pennation in a contracting human muscle *in vivo*. *J. Appl. Physiol.* **82**, 354-358. doi:10.1152/jappl.1997.82.1.354
- Fukunaga, T., Roy, R. R., Shellock, F. G., Hodgson, J. A., Day, M. K., Lee, P. L., Kwong-Fu, H. and Edgerton, V. R.** (1992). Physiological cross-sectional area of human leg muscles based on magnetic resonance imaging. *J. Orthop. Res.* **10**, 926-934. doi:10.1002/jor.1100100623
- Gans, C. and Bock, W. J.** (1965). The functional significance of muscle architecture – a theoretical analysis. *Adv. Anat. Embryol. Cell Biol.* **38**, 115-142.
- Gasser, H. S. and Hill, A. V.** (1924). The dynamics of muscular contraction. *Proc. R. Soc. Lond. Ser. B Biol. Sci.* **96**, 398-437. doi:10.1098/rspb.1924.0035
- Gillis, G. B. and Biewener, A. A.** (2001). Hindlimb muscle function in relation to speed and gait: *in vivo* patterns of strain and activation in a hip and knee extensor of the rat (*Rattus norvegicus*). *J. Exp. Biol.* **204**, 2717-2731.
- Günther, M., Schmitt, S. and Wank, V.** (2007). High-frequency oscillations as a consequence of neglected serial damping in Hill-type muscle models. *Biol. Cybern.* **97**, 63-79. doi:10.1007/s00422-007-0160-6
- Günther, M., Röhrle, O., Haeufle, D. F. and Schmitt, S.** (2012). Spreading out muscle mass within a Hill-type model: a computer simulation study. *Comput. Math. Methods Med.* **2012**, 848630. doi:10.1155/2012/848630
- Hatze, H.** (1977). A myocybernetic control model of skeletal muscle. *Biol. Cybern.* **25**, 103-119. doi:10.1007/BF00337268
- Heerkens, Y. F., Woittiez, R. D., Kiehl, J., Huijting, P. A., Huson, A., van Ingen Schenau, G. J. and Rozendal, R. H.** (1987). Mechanical properties of passive rat muscle during sinusoidal stretching. *Pflügers Arch.* **409**, 438-447. doi:10.1007/BF00583799
- Herzog, W. and Leonard, T. R.** (2002). Force enhancement following stretching of skeletal muscle: a new mechanism. *J. Exp. Biol.* **205**, 1275-1283.
- Herzog, W., Duvall, M. and Leonard, T. R.** (2012). Molecular mechanisms of muscle force regulation: a role for titin? *Exerc. Sport Sci. Rev.* **40**, 50-57. doi:10.1097/JES.0b013e31823cd75b
- Herzog, W., Leonard, T. R. and Wu, J. Z.** (2000). The relationship between force depression following shortening and mechanical work in skeletal muscle. *J. Biomech.* **33**, 659-668. doi:10.1016/S0021-9290(00)00008-7
- Hill, A. V.** (1938). The heat of shortening and the dynamic constants of muscle. *Proc. R. Soc. Lond. B Biol. Sci.* **126**, 136-195. doi:10.1098/rspb.1938.0050
- Hill, A. V.** (1970). *First and Last Experiments in Muscle Mechanics*. Cambridge, UK: Cambridge University Press.
- Hodgson, J. A., Finni, T., Lai, A. M., Edgerton, V. R. and Sinha, S.** (2006). Influence of structure on the tissue dynamics of the human soleus muscle observed in MRI studies during isometric contractions. *J. Morphol.* **267**, 584-601. doi:10.1002/jmor.10421
- Hodson-Tole, E. F., Loram, I. D. and Vieira, T. M. M.** (2013). Myoelectric activity along human gastrocnemius medialis: different spatial distributions of postural and electrically elicited surface potentials. *J. Electromyogr. Kinesiol.* **23**, 43-50. doi:10.1016/j.jelekin.2012.08.003
- Holm, S.** (1979). A simple sequentially rejective multiple test procedure. *Scand. J. Stat.* **6**, 65-70.
- Holt, N. C., Wakeling, J. M. and Biewener, A. A.** (2014). The effect of fast and slow motor unit activation on whole-muscle mechanical performance: the size principle may not pose a mechanical paradox. *Proc. R. Soc. B* **281**, 20140002. doi:10.1098/rspb.2014.0002
- Hothorn, T., Bretz, F. and Westfall, P.** (2008). Simultaneous inference in general parametric models. *Biom. J.* **50**, 346-363. doi:10.1002/bimj.200810425
- James, R. S., Young, I. S., Cox, V. M., Goldspink, D. F. and Altringham, J. D.** (1996). Isometric and isotonic muscle properties as determinants of work loop power output. *Pflügers Arch. Eur. J. Physiol.* **432**, 767-774. doi:10.1007/s004240050197
- Johnson, T. P. and Johnston, I. A.** (1991). Power output of fish muscle fibres performing oscillatory work: effects of acute and seasonal temperature change. *J. Exp. Biol.* **157**, 409-423.

- Josephson, R. K.** (1985). Mechanical power output from striated muscle during cyclic contraction. *J. Exp. Biol.* **114**, 493-512.
- Josephson, R. K.** (1993). Contraction dynamics and power output of skeletal muscle. *Annu. Rev. Physiol.* **55**, 527-546. doi:10.1146/annurev.ph.55.030193.002523
- Josephson, R. K. and Darrell, S. R.** (1989). Strain, muscle length and work output in a crab muscle. *J. Exp. Biol.* **145**, 45-61.
- Josephson, R. K. and Edman, K. A. P.** (1988). The consequences of fibre heterogeneity on the force-velocity relation of skeletal muscle. *Acta Physiol. Scand.* **132**, 341-352. doi:10.1111/j.1748-1716.1988.tb08338.x
- Kinugasa, R., Kawakami, Y., Sinha, S. and Fukunaga, T.** (2011). Unique spatial distribution of *in vivo* human muscle activation. *Exp. Physiol.* **96**, 938-948. doi:10.1113/expphysiol.2011.057562
- Krylow, A. M. and Sandercock, T. G.** (1997). Dynamic force responses of muscle involving eccentric contraction. *J. Biomech.* **30**, 27-33. doi:10.1016/S0021-9290(96)00097-8
- Levin, A. and Wyman, J.** (1927). The viscous elastic properties of muscle. *Proc. R. Soc. Lond. B Biol. Sci.* **101**, 218-243. doi:10.1098/rspb.1927.0014
- Lieber, R. L., Leonard, M. E. and Brown-Maupin, C. G.** (2000). Effects of muscle contraction on the load-strain properties of frog aponeurosis and tendon. *Cells Tissues Organs* **166**, 48-54. doi:10.1159/000016708
- Maden-Wilkinson, T., Degens, H., Jones, D. A. and McPhee, J. S.** (2013). Comparison of MRI and DXA to measure muscle size and age-related atrophy in thigh muscles. *J. Musculoskelet. Neuronal Interact.* **13**, 320-328.
- Maganaris, C. N. and Narici, M. V.** (2005). Mechanical properties of tendons. In *Tendon Injuries-Basic Science and Clinical Medicine* (ed. N. Maffulli, P. Renstrom and W. B. Leadbetter), pp. 14-21. London, UK: Springer.
- Maganaris, C. N., Baltzopoulos, V. and Sargeant, A. J.** (1998). *In vivo* measurements of the triceps surae complex architecture in man: implications for muscle function. *J. Physiol.* **512**, 603-614. doi:10.1111/j.1469-7793.1998.603be.x
- Maréchal, G. and Plaghki, L.** (1979). The deficit of the isometric tetanic tension redeveloped after a release of frog muscle at a constant velocity. *J. Gen. Physiol.* **73**, 453-467. doi:10.1085/jgp.73.4.453
- McGuigan, M. P., Yoo, E., Lee, D. V. and Biewener, A. A.** (2009). Dynamics of goat distal hind limb muscle-tendon function in response to locomotor grade. *J. Exp. Biol.* **212**, 2092-2104. doi:10.1242/jeb.028076
- Meier, P. and Blickhan, R.** (2000). FEM-simulation of skeletal muscle: the influence of inertia during activation and deactivation. In *Skeletal Muscle Mechanics: From Mechanisms to Function* (ed. W. Herzog), pp. 207-233. Chichester, UK: John Wiley & Sons Ltd.
- Meijer, K., Grootenboer, H. J., Koopman, H. F. J. M., van Der Linden, B. J. J. and Huijing, P. A.** (1998). A Hill type model of rat medial gastrocnemius muscle that accounts for shortening history effects. *J. Biomech.* **31**, 555-563. doi:10.1016/S0021-9290(98)00048-7
- Millard, M., Uchida, T., Seth, A. and Delp, S. L.** (2013). Flexing computational muscle: modeling and simulation of musculotendon dynamics. *J. Biomech. Eng.* **135**, 021005. doi:10.1115/1.4023390
- Morgan, D. L., Whitehead, N. P., Wise, A. K., Gregory, J. E. and Proske, U.** (2000). Tension changes in the cat soleus muscle following slow stretch or shortening of the contracting muscle. *J. Physiol.* **522**, 503-513. doi:10.1111/j.1469-7793.2000.t01-2-00503.x
- Morse, C. I., Degens, H. and Jones, D. A.** (2007). The validity of estimating quadriceps volume from single MRI cross-sections in young men. *Eur. J. Appl. Physiol.* **100**, 267-274. doi:10.1007/s00421-007-0429-4
- Perreault, E. J., Heckman, C. J. and Sandercock, T. G.** (2003). Hill muscle model errors during movement are greatest within the physiologically relevant range of motor unit firing rates. *J. Biomech.* **36**, 211-218. doi:10.1016/S0021-9290(02)00332-9
- Pratt, C. A. and Loeb, G. E.** (1991). Functionally complex muscles of the cat hindlimb. I. Patterns of activation across sartorius. *Exp. Brain Res.* **85**, 243-256. doi:10.1007/bf00229404
- Randhawa, A., Jackman, M. E. and Wakeling, J. M.** (2013). Muscle gearing during isotonic and isokinetic movements in the ankle plantarflexors. *Eur. J. Appl. Physiol.* **113**, 437-447. doi:10.1007/s00421-012-2448-z
- Roots, H., Offer, G. W. and Ranatunga, K. W.** (2007). Comparison of the tension responses to ramp shortening and lengthening in intact mammalian muscle fibres: crossbridge and non-crossbridge contributions. *J. Muscle Res. Cell Motil.* **28**, 123-139. doi:10.1007/s10974-007-9110-0
- Ross, S. A. and Wakeling, J. M.** (2016). Muscle shortening velocity depends on tissue inertia and level of activation during submaximal contractions. *Biol. Lett.* **12**, 20151041. doi:10.1098/rsbl.2015.1041
- Ross, S. A., Nigam, N. and Wakeling, J. M.** (2018b). A modelling approach for exploring muscle dynamics during cyclic contractions. *PLoS Comput. Biol.* **14**, e1006123. doi:10.1371/journal.pcbi.1006123
- Ross, S. A., Ryan, D. S., Dominguez, S., Nigam, N. and Wakeling, J. M.** (2018a). Size, history-dependent, activation and three-dimensional effects on the work and power produced during cyclic muscle contractions. *Integr. Comp. Biol.* **58**, 232-250. doi:10.1093/icb/icy021
- Roy, R. R., Meadows, I. D., Baldwin, K. M. and Edgerton, V. R.** (1982). Functional significance of compensatory overloaded rat fast muscle. *J. Appl. Physiol.* **52**, 473-478. doi:10.1152/jappl.1982.52.2.473
- Schieber, M. H.** (1993). Electromyographic evidence of two functional subdivisions in the Rhesus monkey's flexor digitorum profundus. *Exp. Brain Res.* **95**, 251-260. doi:10.1007/BF000229783
- Schoemaker, I., Hoefnagel, P. P. W., Mastenbroek, T. J., Kolff, C. F., Schutte, S., van der Helm, F. C. T., Picken, S. J., Gerritsen, A. F. C., Wielopolski, P. A., Spekrijse, H. et al.** (2006). Elasticity, viscosity, and deformation of orbital fat. *Invest. Ophthalmol. Vis. Sci.* **47**, 4819-4826. doi:10.1167/iov.05-1497
- Shiavi, R. and Griffin, P.** (1983). Changes in electromyographic gait patterns of calf muscles with walking speed. *IEEE Trans. Biomed. Eng.* **30**, 73-76. doi:10.1109/TBME.1983.325171
- Soman, A., Hedrick, T. L. and Biewener, A. A.** (2005). Regional patterns of pectoralis fascicle strain in the pigeon *Columba livia* during level flight. *J. Exp. Biol.* **208**, 771-786. doi:10.1242/jeb.01432
- Stevens, E. D. and Syme, D. A.** (1989). The relative changes in isometric force and work during fatigue and recovery in isolated toad sartorius muscle. *Can. J. Physiol. Pharmacol.* **67**, 1544-1548. doi:10.1139/y89-249
- Stevens, E. D. and Syme, D. A.** (1993). Effect of stimulus duty cycle and cycle frequency on power output during fatigue in rat diaphragm muscle doing oscillatory work. *Can. J. Physiol. Pharmacol.* **71**, 910-916. doi:10.1139/y93-138
- Swoap, S. J., Caiozzo, V. J. and Baldwin, K. M.** (1997). Optimal shortening velocities for *in situ* power production of rat soleus and plantaris muscles. *Am. J. Physiol. Cell Physiol.* **273**, C1057-C1063. doi:10.1152/ajpcell.1997.273.3.C1057
- Syme, D. A.** (1990). Passive viscoelastic work of isolated rat, *Rattus norvegicus*, diaphragm muscle. *J. Physiol.* **424**, 301-315. doi:10.1113/jphysiol.1990.sp018068
- Templeton, G. H. and Nardizzi, L. R.** (1974). Elastic and viscous stiffness of the canine left ventricle. *J. Appl. Physiol.* **36**, 123-127. doi:10.1152/jappl.1974.36.1.123
- Templeton, G. H., Wildenthal, K., Willerson, J. T. and Reardon, W. C.** (1974). Influence of temperature on the mechanical properties of cardiac muscle. *Circ. Res.* **34**, 624-634. doi:10.1161/01.RES.34.5.624
- Thelen, D. G.** (2003). Adjustment of muscle mechanics model parameters to simulate dynamic contractions in older adults. *J. Biomech. Eng.* **125**, 70-77. doi:10.1115/1.1531112
- Tikkanen, O., Haakana, P., Pesola, A. J., Häkkinen, K., Rantalainen, T., Havu, M., Pullinen, T. and Finni, T.** (2013). Muscle activity and inactivity periods during normal daily life. *PLoS ONE* **8**, e52228. doi:10.1371/journal.pone.0052228
- Wakeling, J. M.** (2008). The recruitment of different compartments within a muscle depends on the mechanics of the movement. *Biol. Lett.* **5**, 30-34. doi:10.1098/rsbl.2008.0459
- Wakeling, J. M., Lee, S. S. M., Arnold, A. S., de Boef Miara, M. and Biewener, A. A.** (2012). A muscle's force depends on the recruitment patterns of its fibres. *Ann. Biomed. Eng.* **40**, 1708-1720. doi:10.1007/s10439-012-0531-6
- Wilson, R. S. and James, R. S.** (2004). Constraints on muscular performance: trade-offs between power output and fatigue resistance. *Proc. R. Soc. B* **271**, S222-S225. doi:10.1098/rsbl.2003.0143
- Winters, T. M., Takahashi, M., Lieber, R. L. and Ward, S. R.** (2011). Whole muscle length-tension relationships are accurately modeled as scaled sarcomeres in rabbit hindlimb muscles. *J. Biomech.* **44**, 109-115. doi:10.1016/j.jbiomech.2010.08.033
- Zajac, F. E.** (1989). Muscle and tendon: properties, models, scaling, and application to biomechanics and motor control. *Crit. Rev. Biomed. Eng.* **17**, 359-411.